

# When Worse is Better: Navigating the compression-generation tradeoff in visual tokenization

Vivek Ramanujan<sup>†‡</sup>    Kushal Tirumala<sup>◇</sup>  
 Armen Aghajanyan<sup>‡</sup>    Luke Zettlemoyer<sup>◇†</sup>    Ali Farhadi<sup>†</sup>

<sup>†</sup>University of Washington    <sup>◇</sup>Meta FAIR

<sup>‡</sup> Work done while at Meta FAIR

ramanv@cs.washington.edu

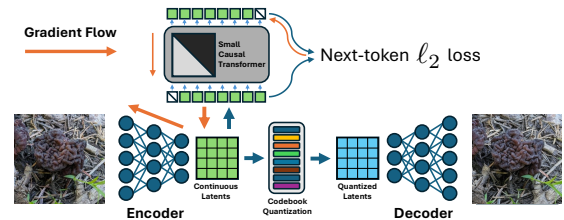
## Abstract

Current image generation methods, such as latent diffusion and discrete token-based generation, depend on a two-stage training approach. In stage 1, an auto-encoder is trained to compress an image into a latent space; in stage 2, a generative model is trained to learn a distribution over that latent space. Most work focuses on maximizing stage 1 performance independent of stage 2, assuming better reconstruction always leads to better generation. However, we show this is not strictly true. Smaller stage 2 models can benefit from more compressed stage 1 latents even if reconstruction performance worsens, showing a fundamental trade-off between compression and generation modeling capacity. To better optimize this trade-off, we introduce Causally Regularized Tokenization (CRT), which uses knowledge of the stage 2 generation modeling procedure to embed useful inductive biases in stage 1 latents. This regularization makes stage 1 reconstruction performance worse, but makes stage 2 generation performance better by making the tokens easier to model: we are able to improve compute efficiency 2-3 $\times$  over baseline and match state-of-the-art discrete autoregressive ImageNet generation (2.18 FID) with half the tokens per image (256 vs. 576) and a fourth the total model parameters (775M vs. 3.1B) as the previous SOTA.

## 1. Introduction

Modern image generation methods use a two-stage approach to training. In the first stage, a model such as a VQGAN [9] (for autoregressive modeling e.g., [54]) or a continuous VAE (for diffusion [40]) is trained to compress images to a latent representation. In the second stage, a generative model is trained to learn a prior over the latent distribution induced by the first stage. Generation is done by using the second stage model to sample a latent, and then applying the decoder of the first stage model to map

### Stage 1: Causally regularized tokenization (CRT)



### Stage 2: Auto-regressive Image Generation

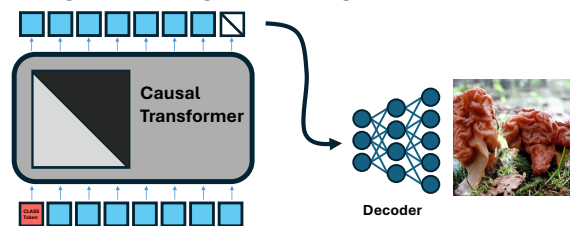


Figure 1. **Overview of our method.** We introduce a small 2-layer causal transformer [8, 35, 46] trained to optimize  $l_2$  next-token prediction on the pre-quantized latents of the auto-encoder. This loss is propagated through the encoder, producing tokens with a causal transformer inductive bias. Thus, we call our method Causally Regularized Tokenization (CRT).

back to image space. This setup reveals an interesting interaction between the stage 1 and stage 2 models. The most important interacting variables for generation performance are: (1) The reconstruction performance of the stage 1 auto-encoder (its “distortion”), (2) The degree of compression of the stage 1 auto-encoder (its “rate”)<sup>1</sup> and (3) The smallest achievable loss of the stage 2 model in learning a distribution over this compressed representation (the “irreducible loss” of distribution modeling). Much empiri-

<sup>1</sup>Note that the concept of “rate” is the entropy of the distribution, so the theoretical lower bound on compression, not the compression ratio we actually achieve.



Figure 2. **Qualitative examples (best viewed zoomed in).** Random, non-curated samples from  $\text{CRT}_{opt}\text{-AR}$  models of increasing scale (111M to 775M parameters, ImageNet 256x256). Larger models demonstrate improved visual fidelity and coherence across diverse subjects including animals, landscapes, and objects across scales. CRT allows for even small models to produce high quality outputs.

cal work has gone into improving (1), as it is generally seen as the lower bound of generation performance. Indeed, scaling laws [15, 19, 23, 59] indicate that stage 2 models can be made arbitrarily powerful and are therefore bottlenecked by stage 1 model performance. But what if our stage 2 model is limited (e.g., by inference time compute limitations)? Given a limited capacity stage 2 model, what is the optimal stage 1 auto-encoder? We view this as a trade-off between rate, distortion, and distribution modeling. Reducing the rate also increases the distortion but would improve distribution modeling performance because the irreducible loss is lower-bounded by rate. We hypothesize that optimizing this trade-off between distortion and distribution modeling would yield substantial generation improvements and enable parameter-efficient stage 2 training.

We study this in the context of a vector-quantized GAN (VQGAN) stage 1 model and an auto-regressive stage 2 model trained on VQ tokens. We explore key interventions which affect the stage 1 rate: **(a)** Number of tokens per image, **(b)** Dictionary size of the VQ model, and **(c)** Data scaling, and examine how they affect stage 2 generation performance as a function of model scale. We show that small models benefit strongly from more compressed representations, and that this relationship also depends on stage 2 data scale. Given these findings, we ask: *Can we design an optimal stage 1 tokenizer given that we know our stage 2 model is auto-regressive?* Through a simple model-based causal loss, we learn a causal inductive bias on our stage 1 tokenizer. Intuitively, our loss attempts to make token  $i$  as predictable as possible given tokens 0 through  $i - 1$ . We call this training recipe Causally Regularized Tokenization (CRT). When equal training compute is used for stage 1, this regularization makes reconstruction performance worse, but improves stage 2 generation performance across ImageNet [41] and LSUN [52]. With CRT, we also show significant improvements in stage 2 model performance scaling, especially for small models.

### Summary of major contributions.

- We study the complex trade-off between compression and generation by varying codebook size, tokens per image, and stage 2 training compute. Our analysis shows that the ideal amount of image compression varies with generation

model capacity, challenging conventional wisdom about reconstruction quality.

- We provide a principled framework for analyzing this trade-off through the lens of scaling laws, showing consistent patterns across multiple orders of magnitude in computational budget.

- We introduce a method for training a stage 1 tokenizer with a causal inductive bias. This improves inference and training compute scaling of our stage 2 models, without any other interventions, leading to our key result: by making tokens easier to model, we improve compute efficiency 2-3x over baseline. We also match SOTA discrete autoregressive ImageNet generation (2.18 FID) with half the tokens per image (256 vs 576) and a third the total model parameters (740M vs. 3.1B) as the previous SOTA model [43].

## 2. Related Work

**Evolution of visual tokenization.** The current paradigm of discrete visual tokenizers came from VQ-VAE [49], originally introduced as a method for discrete latent representation learning in continuous domains such as image and audio. It was introduced to prevent the posterior collapse problem in VAEs by separating the compression and generation phases of training. Section 4.2 of [49] notes that their loss function leads to blurry reconstructions, and the authors suggest including perceptual metrics (metrics that align with human judgment of similarity) in the loss function. Esser et al. [10] explores this idea with VQGAN, which introduces a perceptual loss based on *LPIPS* [58], and a GAN loss to add realistic textures. Since the advent of VQGAN, there have been numerous attempts at improving visual tokenizers [14, 22, 34, 38, 39, 50, 51, 53, 57, 60–62]. Some works focus on improvements including ViT-VQGAN [53], which replaces CNN layers with ViT layers, and MoVQGAN [61], which adds adaptive instance normalization layers in the CNN decoder. Other works focus on mitigating “codebook collapse” [20] in vector quantization (VQ) [13] by introducing novel quantization schemes, for example by replacing dead codes with encoder outputs [7]. We refer the reader to [20] for a thorough review of these methods. Other works replace VQ entirely with scalar quantization techniques [32], and demonstrates increased

codebook utilization compared to VQ: for example, MAG-VIT [31, 55] quantizes each dimension to 2 values and adds entropy loss to encourage codebook utilization.

**Trade-offs between stage 1 and stage 2 performance.** We are not the first to notice a disconnect between stage 1 and stage 2 performance. [47] extensively studies how different regularization methods affect the usefulness of learned VAE representations for downstream representations, introducing the “rate-distortion-usefulness” trade-off. Notably, they highlight that stage 1 loss (e.g. VAE loss) is not representative of downstream task usefulness. [48] also shows in Figure 4 demonstrates that increasing  $\beta$  in their  $\beta$ -VAE [17] architecture worsens reconstruction but improves generation performance. Recent advances in lookup-free quantization [32, 55] have unlocked better codebook utilization, improving stage 1 performance. Both works observe that scaling up codebook size improves stage 1 performance but degrades stage 2 performance (see Figure 3 in [32] and Figure 1 in [55]). Outside of visual tokenization, previous work in text tokenization observes that optimizing text tokenizer compression (i.e. stage 1 performance) leads to worse perplexity [28] and downstream accuracy [42].

### 3. Experiments & Methodology

**Structure of our study.** Our goal is to understand the variables involved in tokenizer construction affecting generation performance at different model scales. First, fixing a stage 1 tokenizer, we rigorously study the connection between generation performance and compute scaling, establishing gFID on ImageNet as a consistent generation metric to center our study.<sup>2</sup> At the core of this exploration is the rate-distortion trade-off in the stage 1 tokenizer. How does changing the stage 1 “rate” (bits per output pixel) affect stage 2 model performance at various scales? We study scaling properties with respect to key tokenizer interventions which affect this rate-distortion trade-off. Finally, we study a new angle on the rate-distortion which affects compute-optimal generation performance scaling: causally regularized tokenization (CRT).

#### 3.1. VQGAN and Auto-regressive Image Generation

We summarize the common auto-regressive image generation procedure we use for the basis of our study [9, 43, 54].

**Stage 1 (Tokenization).** In this stage, the goal is to map an image  $x \in \mathbb{R}^{H \times W \times 3}$  to a set of  $N$  discrete tokens  $X_i \in \mathcal{C}$ , where  $\mathcal{C}$  is a codebook such that  $\mathcal{C} \subset \mathbb{R}^d$ . We also learn a decoder which can reconstruct the original image from a set of tokens. We use the VQGAN architecture [9], which is a ResNet-based architecture that is a mix of convolutions and

<sup>2</sup>This consistency is not as present when using gFID on non-ImageNet datasets because the Inception network [44] is in-distribution on ImageNet.

self-attention layers in both the encoder and decoder. During training, the encoder maps the input image  $x$  to continuous latents  $\hat{X}_i$ . Then, we use a codebook look-up to determine the nearest embedding  $X_i \in \mathcal{C}$ . Finally, these are passed to the decoder to get a reconstruction.

**Stage 2 (Generation).** In this stage, the goal is to learn a prior over the latent tokens learned in the previous stage. For each image in our train set, we use the encoder learned in stage 1 to map it to a set of discrete tokens. We fix an order with which to decode these tokens per image (raster-scan works best empirically), and treat these as sequences. Finally, we train a transformer with causal attention to learn the conditional distributions  $p(x_i|x_0 \dots x_{i-1})$  for all tokens  $x_i$  by maximizing  $\prod_{i=0}^N q_\theta(x_i|x_0 \dots x_{i-1})$  for our model  $q_\theta$ . This is done by minimizing cross-entropy loss over the next-token prediction objective. We train our generation models in the class-conditional regime. To do this, we append a learned class token to the start of the sequence. We also use classifier-free guidance (CFG) at inference time, where we predict a token based on both the class-conditional and unconditional distributions. These decisions are discussed in detail in Section 3.6. Details on architecture, training, and CFG discussed in Appendix A.

**Data.** We train and evaluate primarily on ImageNet (1.28M images, 1000 classes) for class-conditional generation without introducing external data for both stage 1 and stage 2. To confirm general applicability of our method to large scale datasets, we also evaluate our results on several categories of the Large-Scale Scene Understanding Dataset. These categories are cats (1.66M images), horses (2.0M images), and bedrooms (3.02M images).

#### 3.2. Metrics

The two categories for evaluation are reconstruction performance (to evaluate the stage 1 model) and generation performance (to evaluate the stage 2 + stage 1 pipeline).

**Reconstruction metrics.** We use Fréchet Inception Distance (FID) [16] between validation and a reconstructed validation set as our primary metric. We refer to this metric as rFID (reconstruction FID). We also report the signal-to-noise ratio (PSNR) and the multi-scale structured similarity metric (MS-SSIM) [1].

**Generation metrics.** We use FID between the generations and the whole validation set for our primary metric. For clarity, we refer to this as generation FID (gFID). To conform with existing literature, we use the OpenAI guided diffusion [6] repository to evaluate our models. We report Inception Score, precision, and recall, which are proxies for generation fidelity and diversity.

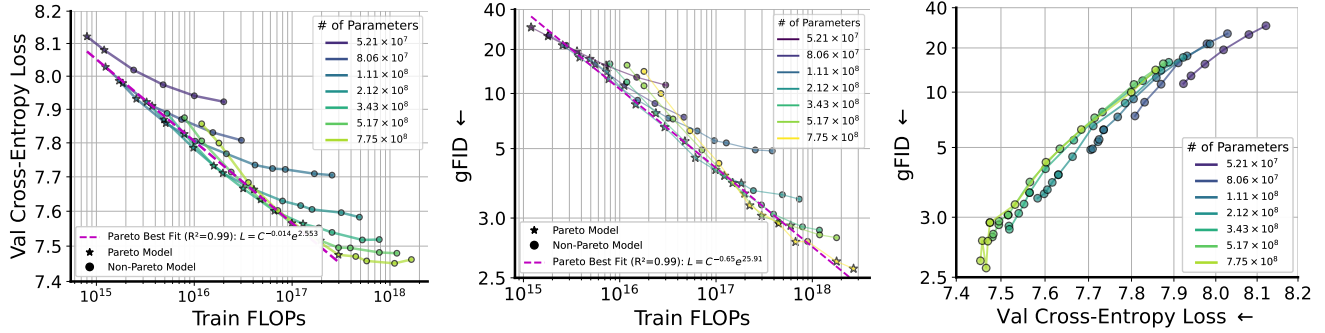


Figure 3. **Neural scaling laws for auto-regressive image generation (ImageNet 256x256).** We show validation cross-entropy loss (left) and gFID (center) as a function of total train FLOPs. Across model scales, we observe log-log linear scaling with train FLOPs for both FID and cross-entropy loss across Pareto frontiers. Moreover, we observe validation cross entropy loss is generally predictive of gFID (right). However, at large model scales (yellow-line), we notice that over-training can lead increase in validation cross-entropy but decrease in gFID, implying that validation loss is predictive of gFID only when training duration is held consistent (see Section 3.3.1).

### 3.3. Validation Loss and Generation Performance

#### 3.3.1. Neural Scaling Laws for Image Generation

**Setup.** We fix a stage 1 tokenizer (16k token codebook size, 256 sequence length), vary stage 2 model parameters and compute dedicated to training. Fixing codebook size is important because, all else being equal, validation cross-entropy loss is proportional to the intrinsic entropy of the codes, which increases log-log-linearly by codebook size (see Figure 10). We only plot the end point of each training run since our cosine learning rate decay schedule results in substantial validation loss changes in the last few iterations of training, yielding inconsistent scaling trends. Given that we are iterating on a fixed-size dataset (about  $3 \times 10^8$  total tokens at 256 tokens per image), we do not scale models past 740M parameters to avoid data scale bottlenecks.

**Log-log-linear scaling for image generation.** In Figure 3, we present our findings on the relationship between compute scaling and generation performance. These results corroborate scaling trends found in [15, 23]. We see consistent log-log-linear scaling with validation loss (Figure 3 (left)) on the compute validation loss Pareto curve across four orders of magnitude. These validation scaling loss trends serve as the basis for our scaling studies.

**Validation loss and generation performance.** In Figure 3 (center), we plot the gFID score as a function of training compute for different model scales. We see that, in general, lower validation loss implies better generation performance (lower gFID). However, if we look at the upper Pareto frontier for Figure 3 (left) (highest gFID score for lowest validation loss), we see that individual model scales achieve lower gFID for correspondingly higher validation losses. This is considered the “overtraining” regime with respect to validation loss, described in [12]. This implies that *validation loss is only predictive of FID when the number of training steps is held constant*. Therefore, compute optimality with respect to validation loss also corresponds to

compute optimality with respect to gFID, meaning overall scaling bounds transfer, even if specific trends do not.

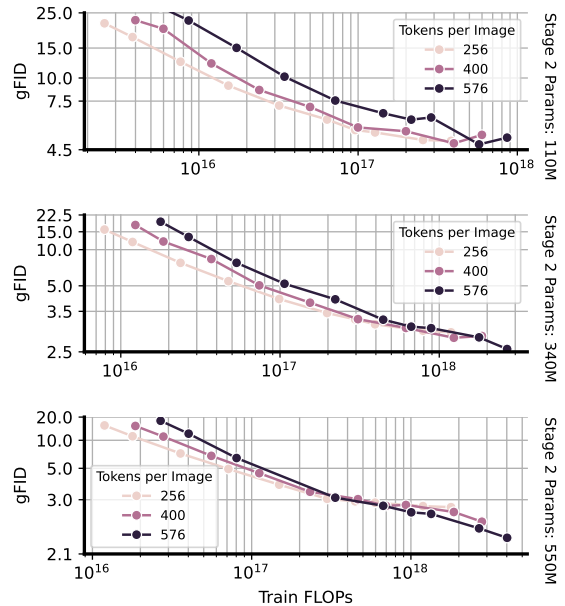


Figure 4. **Relationship between tokens per image and model size.** We show compute scaling laws for stage 2 performance for different stage 1 tokens/image. Each plot uses a different stage 2 model size (left: 110M, center: 340M, right: 550M) trained across several durations (separate training runs). We notice that larger models can take advantage of more tokens/image, whereas smaller models are more compute efficient fewer tokens.

### 3.4. Sequence Length and Compute Scaling

In this section, we investigate how scaling the number of tokens per image affects the rFID and gFID.

**Setup.** To vary the number of tokens per image, we follow [43] to re-use our tokenizers trained at  $256 \times 256$  resolution and evaluate them at higher resolutions. Our base tokenizers trained use a downsample factor of 16: if we

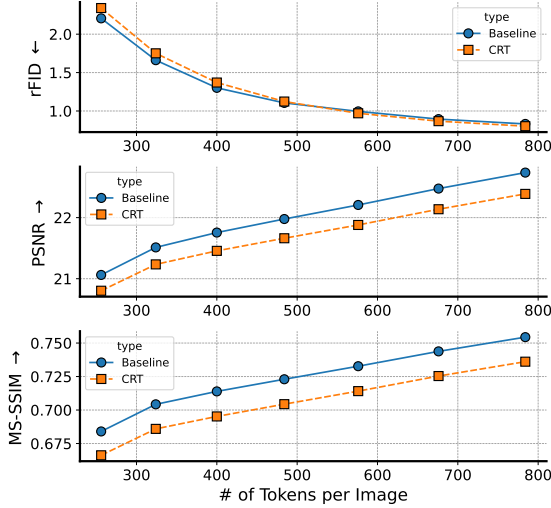


Figure 5. **Performance improves reliably with increase tokens/image.** We demonstrate the results of a simple sweep of tokens/image across our three main reconstruction metrics. Our base model is trained with 256 tokens/image (16k codebook size), and we increase the tokens/image at inference time using the method described in Section 3.4. We observe that increasing tokens/image consistently improves reconstruction performance. We also show the performance of CRT tokens, which has the worse (reconstruction) but better (generation) phenomena.

process an  $R \times R$  image, the number of tokens produced is  $(R/16)^2 = R^2/256$ . To measure rFID and PSNR, we then take the  $R \times R$  output and downsize to  $256 \times 256$  with bicubic interpolation. In Figure 5 we observe the expected result that increasing sequence length improves reconstruction performance. We opt for this method as opposed to changing the number of downsample layers in the stage 1 tokenizer (e.g. [9, 27, 61]) to avoid introducing a confounding variables related to architectural changes.

**Model Capacity and Sequence Length.** In Figure 4, we study how performance scaling changes as a result of both sequence length and stage 2 model size. We vary the training iterations at three model scales, 111M, 340M, and 550M parameters and study how the number of tokens per image affects generation performance. We see that for smaller models, training with a lower number of tokens per image is more compute efficient, whereas larger models can take advantage of the greater representation capacity of longer sequence lengths. The exact training parameters and full pareto curves for these experiments can be found in the appendix. Notably in those results, we find that increasing sequence lengths makes the compute optimal Pareto curve *worse* above the 256 token/image rFID lower bound.

### 3.5. Codebook Size and Compute Scaling

Codebook size is the second mechanism for changing the rate of the image tokenizer. This differs from changing sequence length because it has a minor effect on inference

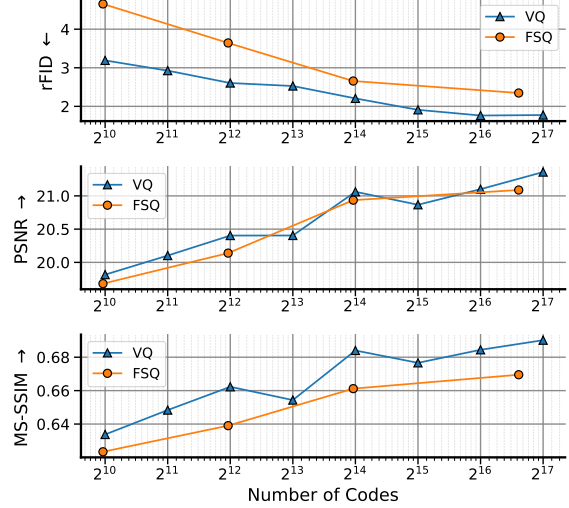


Figure 6. **Codebook reconstruction performance scaling.** We observe that reconstruction performance reliably improves as we increase codebook size across all metrics. We compare vector quantization (VQ, orange) with finite scalar quantization (FSQ, blue), a popular recent “lookup-free” method. In contrast to prior work, we find that with a good codebook recipe, VQ uniformly outperforms FSQ and scales to  $>100k$  codes.

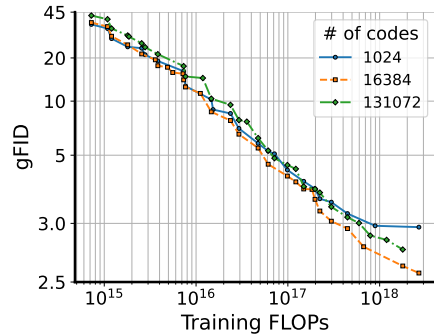


Figure 7. **Pareto-optimal image-generation compute curves for different codebook sizes:** We plot the pareto-optimal compute curves for stage 2 performance for different codebook sizes (1k, 16k, and 131k). In the low-compute regime ( $10^{15}$  FLOPs), we observe that the 1k codebook outperforms the 131k by 5-10 gFID; in the high compute regime ( $10^{18}$  FLOPs), we observe the reverse effect. Notably, the 16k codebook consistently matches or outperforms 1k and 131k at every compute scale, indicating a sweet spot for codebook size. Full scaling plots are in the appendix.

cost, both for the stage 1 and stage 2 models. Changing sequence length increases inference cost quadratically in stage 2 and linearly in stage 1, so the effect is more subtle.

**Stage 1 scaling by codebook size.** In Figure 6, we find consistent improvements in stage 1 rFID, PSNR, and MS-SSIM without collapse in performance, in contrast to prior work [9, 32, 55]. We credit this scaling improvement to modern VQ recipes [43, 53] in conjunction with a long learning rate warm-up period (training recipe details can be found in the appendix). Notably, the gap for rFID between the extremes of our exploration (1k and 131k) is 1.3 rFID.

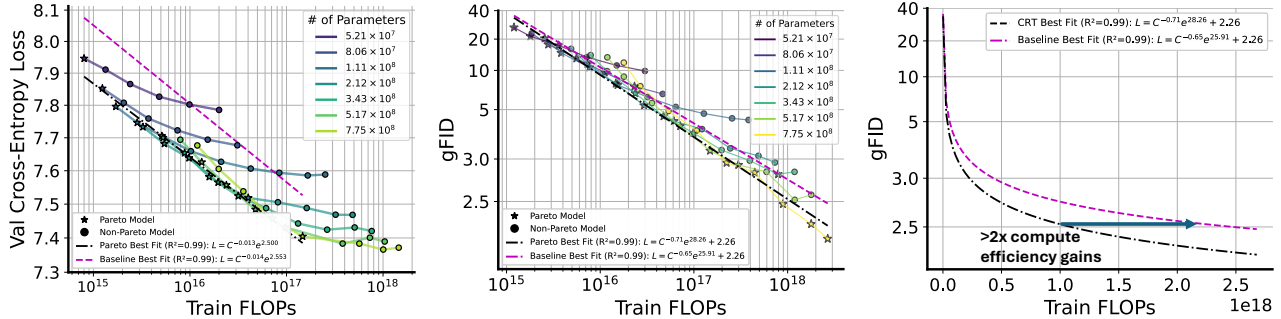


Figure 8. **Stage 2 compute scaling laws with CRT tokens (ImageNet 256x256)**. We demonstrate the superior scaling of CRT tokens across four orders of magnitude with respect to validation cross entropy (**left**) and FID (**center**). The trade-off between reconstruction performance and causal dependence means that CRT has worse reconstruction (2.36 rFID vs 2.21 for the baseline) but yields better stage 2 performance across many model scales. The result is a tokenizer that has better absolute generation performance for per parameter scale, and gets the same performance with  $1.5\times$  to  $2.5\times$  fewer training FLOPs (when comparing pareto frontiers).

**Comparison with finite-scalar quantization [32]**. In Figure 6, compare VQ to FSQ, which is an increasingly popular “lookup-free” quantization scheme across the recommended settings. We find that with a good VQ training recipe, FSQ is outperformed at all codebook scales in both stage 1 and stage 2, in contrast to the results demonstrated in [25, 32]. As a result, we primarily use VQ in this work.

**Stage 2 model scale and codebook size**. In Figure 7, we plot the Pareto frontiers for the extremes of the codebook sizes we study (1k and 131k), along with our baseline codebook size of 16k. We only show the Pareto frontiers for clarity but plot the full model scaling curves in the appendix. When we use less training compute, we see that the 1k codebook outperforms 131k codebook by 5-10 gFID, even though the rFID is significantly lower. At the other extreme, 131k outperforms 1k, as the stage 2 model nears the gFID saturation point and the worse rFID becomes a bottleneck. This crossover happens around  $10^{17}$  train FLOPs. It’s worth noting that the 16k codebook size outperforms both at almost every compute scale, implying that there is an optimal point for the rFID/gFID trade-off.

### 3.6. Causally Regularized Tokenization

We showed that stage 2 model capacity is important when designing a stage 1 tokenizer. Going past capacity, since we know our stage 2 model is an auto-regressive transformer, can we imbue this inductive bias into the tokenizer?

**Setup**. Figure 8 demonstrates our key intervention. We apply an  $\ell_2$  loss parameterized by a causal transformer to the tokens *before* quantization, and backpropagate this loss to the encoder of the our stage 1 auto-encoder. We train with this model-based loss ( $\mathcal{L}_{CRT}$ ) in conjunction standard VQGAN losses, using the same hyperparameters as our baseline recipe. Applying this loss with cross-entropy after quantization is intuitive, however we found this unstable since VQ tokens change drastically during training. We use a 2-layer causal transformer with the architecture of our

stage 2 model. This introduces a 5% cost in training FLOPs, which we control for by training 5% less (2 fewer epochs). For both our baseline and CRT models we use a codebook of size 16k and 256 tokens per image.

**Effects on stage 1 reconstruction**. After applying this loss, our tokenizer is worse in terms of reconstruction against the compute normalized baseline (Figure 5). This is expected behavior. Intuitively, our loss attempts to make token  $i$  as predictable as possible given tokens 0 through  $i - 1$ . The most predictable set of tokens would be if the encoder outputs a sequence of entirely dependent tokens (e.g., the constant token). However, this reduces the total information that can be conveyed through the tokens. Our CRT loss (a proxy for generation) conflicts with reconstruction, implying a trade-off. With this inductive bias, stage 2 scaling is greatly improved, especially at small to medium scales.

**Improvements in stage 2 performance**. In Figure 8, we show the relative scaling properties of stage 2 models using our CRT tokenizer compared to the VQ-GAN baseline (in Figure 3). For clarity, we also include Pareto frontier scaling trends from Figure 3. Figure 8 (**left**) Shows that stage 2 models trained with our tokenizer achieve lower validation losses. Figure 8 (**center**) shows that this translates to improvements generation performance on the training compute Pareto front. Finally, Figure 8 (**right**) shows the actual magnitude of improvement, which the log-log-linear plots obfuscate: CRT achieves gFID scores with  $1.5 - 3\times$  compute efficiency and improve over the baseline, even with worse rFID. We demonstrate non-cherry-picked qualitative outputs from these models in the appendix. We show comparisons at individual model scales in Table 2, and detailed comparisons across training durations in the appendix.

**LSUN [52]**. We demonstrate our method’s generality by evaluating several LSUN categories. We do not reproduce the full scaling study due to computational cost, but in Table 3 we demonstrate improvements in gFID and CLIP [36] gFID across three model scales using CRT. Note that we

Table 1. **System-level comparison between methods on ImageNet 256x256**: We compile results from previous work that report stage 2 autoregressive image generation scores. Our tokenizer method (CRT) generally outperforms other methods when matching number of parameters of the image generation model. CRT<sub>opt</sub> refers to our hyperparameter-tuned CRT tokenizer.

Type	Model	#Para	Tok/Im↓	FID↓	IS↑	Pre↑	Rec↑
Diff.	ADM [6]	554M	–	10.94	101.0	0.69	0.63
Diff.	LDM-4-G [40]	400M	–	3.60	247.7	–	–
Diff.	DiT-L/2 [33]	458M	–	5.02	167.2	0.75	0.57
Diff.	DiT-XL/2 [33]	675M	–	2.27	278.2	0.83	0.57
Diff.	MAR-H [30]	943M	–	1.55	303.7	0.81	0.62
Mask.	MaskGIT [3]	227M	256	6.18	182.1	0.80	0.51
Mask.	RCG (cond.) [29]	502M	256	3.49	215.5	–	–
VAR	VAR-d16 [45]	310M	680	3.30	274.4	0.84	0.51
VAR	VAR-d20 [45]	600M	680	2.57	302.6	0.83	0.56
VAR	VAR-d24 [45]	1.0B	680	2.09	312.9	0.82	0.59
VAR	VAR-d30 [45]	2.0B	680	1.92	323.1	0.82	0.59
AR	VQVAE-2 [37]	13.5B	5120	31.11	~45	0.36	0.57
AR	VQGAN [9]	227M	256	18.65	80.4	0.78	0.26
AR	VQGAN [9]	1.4B	256	15.78	74.3	–	–
AR	VQGAN-re [9]	1.4B	256	5.20	280.3	–	–
AR	ViTVQ [53]	1.7B	1024	4.17	175.1	–	–
AR	RQTran. [27]	3.8B	256	7.55	134.0	–	–
AR	LlamaGen-B [43]	111M	256	6.10	182.54	0.85	0.42
AR	LlamaGen-L [43]	343M	256	3.80	248.28	0.83	0.51
AR	LlamaGen-XL [43]	775M	256	3.39	227.08	0.81	0.54
AR	LlamaGen-XXL [43]	1.4B	256	3.09	253.61	0.83	0.53
AR	LlamaGen-B [43]	111M	576	5.46	193.61	0.83	0.45
AR	LlamaGen-L [43]	343M	576	3.07	256.06	0.83	0.52
AR	LlamaGen-XL [43]	775M	576	2.62	244.08	0.80	0.57
AR	LlamaGen-XXL [43]	1.4B	576	2.34	253.90	0.80	0.59
AR	LlamaGen-3B [43]	3.1B	576	2.18	263.33	0.81	0.58
AR	CRT-AR-111M	111M	256	4.34	195.33	0.81	0.52
AR	CRT-AR-340M	340M	256	2.75	265.24	0.83	0.54
AR	CRT-AR-775M	775M	256	2.35	259.12	0.81	0.59
AR	CRT <sub>opt</sub> -AR-111M	111M	256	4.23	194.87	0.84	0.49
AR	CRT <sub>opt</sub> -AR-340M	340M	256	2.45	249.08	0.82	0.57
AR	CRT <sub>opt</sub> -AR-775M	775M	256	2.18	268.38	0.82	0.58
(validation data)				1.78	236.9	0.75	0.67

Table 2. **Compute-controlled comparison against tuned VQGAN baseline on ImageNet**: We show image generation performance when we control all compute factors (train and test FLOPs for both stage 1 and stage 2 models, with stage 2 trained to saturation, 16k codebook size). Across stage 2 model sizes we observe that CRT is generally superior, indicating that tokens with causal-regularization are more amenable to stage 2 auto-regressive training. See Figure 8 for a comprehensive sweep.

Tok. Type	#Params	Tok/Im	gFID↓	IS↑	Pre↑	Rec↑
Baseline (2.21 rFID)	111M	256	4.90	180.65	0.82	0.51
	211M	256	3.32	251.93	0.84	0.52
	340M	256	2.89	253.25	0.83	0.54
	550M	256	2.77	277.53	0.83	0.56
	740M	256	2.55	242.23	0.80	0.60
CRT (ours) (2.36 rFID)	111M	256	4.34	195.33	0.81	0.52
	211M	256	2.94	241.95	0.83	0.55
	340M	256	2.75	265.24	0.83	0.54
	550M	256	2.55	278.29	0.80	0.59
	740M	256	2.35	259.12	0.81	0.59

use CLIP gFID because these datasets are out of distribution for the Inception network, making FID a more noisy metric. We see a consistent improvement across all model scales.

**Optimizing for absolute performance.** In the previous

Table 3. **Compute-controlled comparison against tuned VQGAN across different datasets**: We provide compute-controlled comparison against our tuned VQGAN baseline (16k codebook size) for different training sets. Similar to Table 2, we observe that CRT generally outperforms a tuned VQGAN baseline.

Dataset	Tok. Type	#Params	Tok/Im	gFID↓	gFID <sub>clip</sub> ↓	Prec↑	Rec↑
LSUN Cats	Baseline (1.35 rFID)	111M	256	5.77	8.14	0.58	0.56
		340M	256	5.21	7.37	0.58	0.58
		740M	256	5.31	6.72	0.59	0.59
	CRT (ours) (1.48 rFID)	111M	256	5.32	7.22	0.60	0.54
		340M	256	4.98	6.77	0.61	0.56
		740M	256	5.32	6.74	0.60	0.57
LSUN Horses	Baseline (1.65 rFID)	111M	256	3.19	5.56	0.62	0.62
		340M	256	3.00	5.09	0.62	0.62
		740M	256	2.56	4.92	0.62	0.63
	CRT (ours) (1.83 rFID)	111M	256	2.65	5.20	0.61	0.61
		340M	256	2.62	4.63	0.61	0.63
		740M	256	2.76	4.05	0.61	0.63
LSUN Bedrooms	Baseline (0.99 rFID)	111M	256	2.57	9.81	0.59	0.53
		340M	256	2.51	9.61	0.58	0.55
		740M	256	2.53	9.50	0.57	0.57
	CRT (ours) (1.39 rFID)	111M	256	2.37	9.06	0.60	0.53
		340M	256	2.08	8.56	0.59	0.56
		740M	256	2.22	8.50	0.58	0.57

sections, we perform compute-controlled comparisons of CRT and baseline. In this section, we apply simple optimizations from literature to our tokenizer to push the limits of our method. These include: (1) increasing training duration from 38 epochs to 80 epochs, (2) doubling the size of the decoder, (3) increasing the codebook size from 16k to 131k (which improves performance for CRT but not our baseline). With these changes, our tokenizer achieves **1.21 rFID**. Our stage 2 training procedures remain constant. In Table 1, we show a system-level comparison of our method (CRT<sub>opt</sub>-AR) to other existing methods in the field. The closest comparison to our method is LlamaGen, which uses the same architectures and inference method. Notably, we exceed the performance of the LlamaGen 3.1B parameter model with our 775M parameter model, while using half the number of tokens per image. This is an **8x reduction** in inference compute. We show non-cherry-picked qualitative examples from select object categories in Figure 2.

**Ablations.** There are two key choices involved with our causal loss: (1) the size of the causal model used during stage 1 training and (2) the weight  $\lambda$  we assign to the  $\ell_2$  next-token prediction loss ( $\lambda\mathcal{L}_{CRT}$ ). We include an ablation of these parameters in Figure 9. We plot the relationship of rFID and gFID with respect to these parameters, computing gFID over an average of 4 stage 2 model scales (80M, 111M, 211M, 340M) trained for 250k iterations each. In Figure 9 (top), we increase the number of layers in our causal regularizer. For every 2-layers we add, we reduce the overall training time by 5% to compensate. We see that rFID uniformly increases with more layers, as expected. After 4 layers, this worsening rFID hurts average gFID. Thus, we chose to use two layers in all of our experiments, which has the added advantage of being very computationally cheap. In Figure 9 (bottom), we see a similar trend. Increasing  $\lambda$  biases the encoder to

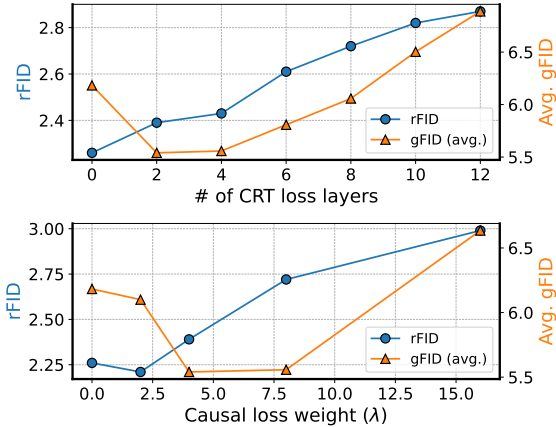


Figure 9. **Impact of CRT hyperparameter choices on reconstruction FID (rFID) and generation FID (gFID).** (top): Increasing the number of causal regularizer layers worsens rFID and, beyond 4 layers, also degrades gFID. (bottom): Higher causal loss weights ( $\lambda$ ) trade off rFID for improved next-token prediction, with optimal balance at  $\lambda = 4$ . 0 layers and  $\lambda = 0$  correspond to baseline. Further discussion in Section 3.6.

focus on making representations easy for next-token prediction rather than reconstruction, making overall rFID worse. However, there’s a sweet spot around  $\lambda = 4$  where this worsened reconstruction is within acceptable range and this also improves overall generation performance.

## 4. Analysis

**Factors affecting validation loss.** We saw that changing the number of tokens per image (Section 3.4) affected compute scaling more significantly than changing the codebook size (Section 3.5). Why is that? We note that for a unigram model, the loss lower bound is the empirical entropy of the codebook distribution per-position, since cross-entropy can be decomposed into  $H(X) + D_{KL}(q(X)|p(X))$  and  $D_{KL} \rightarrow 0$  when  $q \rightarrow p$ . In Figure 10 (top left), we measure this directly over the ImageNet train set over various codebook sizes.<sup>3</sup> In Figure 10 (top right), we see that the average entropy per position *converges*, even as the overall codebook entropy increases log-linearly (as one would expect with 100% codebook utilization), implying that as codebook size increases, codes become more specialized by position. This has the secondary effect of ensuring that the lower bound for a unigram model over these tokens also does not increase, meaning that our stage 2 model can still learn even with very large codebook sizes.

**What does CRT do?** The lower-bound for an  $n$ -gram model is upper-bounded by this estimate, as  $H(X_i) \geq H(X_i|X_0 \dots X_{i-1})$ .  $H(X_i|X_0 \dots X_{i-1})$  is not directly measurable. In fact, this is what we are trying to estimate with language modeling. So we directly model and mini-

<sup>3</sup>Note the periodicity, implying that positions near the center of the image have higher entropy.

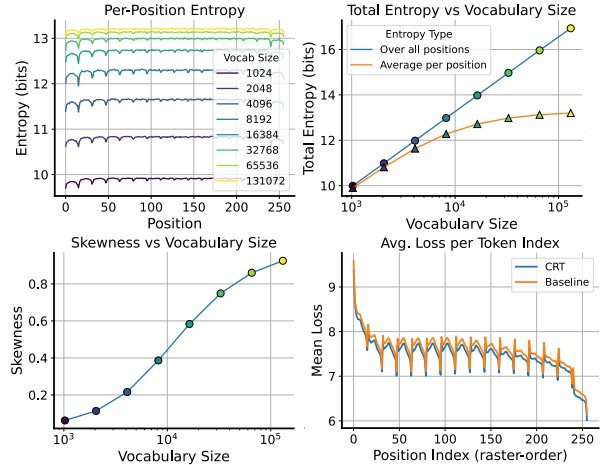


Figure 10. **Entropy analysis of image tokenizers with varying codebook sizes.** (top left) Per-position token entropy following raster scan order, showing higher entropy at image centers and lower at edges. (top right) Global token distribution approaches uniform (diagonal), while per-position expected entropy shows systematic deviation. (bottom left) Distribution skew metric ( $1 - \frac{2^{\text{per position entropy}}}{2^{\text{total entropy}}}$ ) reveals optimal global codebook usage but convergent local usage as codebook size increases, allowing effective stage 2 causal model training. (bottom right) Effects of CRT tokenization uniformly reduce stage 2 loss across all positions. See Section 4 for more details.

mize this in stage 1 with CRT, using the same architecture as in stage 2, to ensure that our inductive biases transfer. In Figure 10 (bottom right), we plot the stage 2 losses per-position for a 211M parameter auto-regressive model between our baseline tokenizer and CRT. These tokenizers have the same codebook size, utilization, and per-position entropy. However, we see that CRT lowers loss uniformly across token positions, with most of the loss reduction happening at the end of the sequence. This implies that the CRT tokenizer has less estimated entropy<sup>4</sup>.

## 5. Conclusion & Future Work

We systematically study the tradeoff between compression and generation for image tokenization and reveal several key insights: First, we demonstrate that the relationship between compression and generation quality is nuanced: smaller models actually benefit from more aggressive compression, even at the cost of reconstruction fidelity. Second, we provide a principled framework for analyzing this trade-off through the lens of scaling laws, showing consistent patterns across multiple orders of magnitude in computational budget. Finally, we introduce Causally Regularized Tokenization (CRT), a method for optimizing tokenizers specifically for autoregressive generation. We introduce a causal inductive biases during tokenizer training

<sup>4</sup>Note that the variance of the model’s final loss is very low ( $\leq 10^{-3}$ ), so this is a significant phenomenon (Figure 8).



which substantially improves compute efficiency (2-3x) and parameter efficiency (4x reduction) compared to previous approaches. Notably, these gains are most pronounced in the resource-constrained regime, making the method particularly valuable for practical applications. Our results highlight the importance of considering the interaction between different components for multi-stage machine learning pipelines: rather than optimizing each stage independently, we achieve significant gains by baking in inductive biases in early stages. This principle suggests several promising directions for future work, for example extending to other architectures (e.g. diffusion models) or other modalities (e.g. video and audio tokenizers).

## References

- [1] Multiscale structural similarity for image quality assessment. In *The Thirty-Seventh Asilomar Conference on Signals, Systems & Computers, 2003*, volume 2, pp. 1398–1402. Ieee, 2003. 3
- [2] Martin Arjovsky, Soumith Chintala, and Léon Bottou. Wasserstein gan. *arXiv preprint arXiv:1701.07875*, 2017. 12
- [3] Huiwen Chang, Han Zhang, Lu Jiang, Ce Liu, and William T Freeman. Maskgit: Masked generative image transformer. In *Proceedings of the IEEE/CVF Conference on Computer Vision and Pattern Recognition*, pp. 11315–11325, 2022. 7
- [4] Xi Chen, Xiao Wang, Soravit Changpinyo, AJ Piergiovanni, Piotr Padlewski, Daniel Salz, Sebastian Goodman, Adam Grycner, Basil Mustafa, Lucas Beyer, et al. Pali: A jointly-scaled multilingual language-image model. *arXiv preprint arXiv:2209.06794*, 2022. 12
- [5] Mostafa Dehghani, Josip Djolonga, Basil Mustafa, Piotr Padlewski, Jonathan Heek, Justin Gilmer, Andreas Steiner, Mathilde Caron, Robert Geirhos, Ibrahim Al-abdulmohsin, et al. Scaling vision transformers to 22 billion parameters. *arXiv preprint arXiv:2302.05442*, 2023. 12
- [6] Prafulla Dhariwal and Alex Nichol. Diffusion models beat gans on image synthesis. *arXiv preprint arXiv:2105.05233*, 2021. 3, 7
- [7] Prafulla Dhariwal, Heewoo Jun, Christine Payne, Jong Wook Kim, Alec Radford, and Ilya Sutskever. Jukebox: A generative model for music. *arXiv preprint arXiv:2005.00341*, 2020. 2
- [8] Alaaeldin El-Nouby, Michal Klein, Shuangfei Zhai, Miguel Angel Bautista, Alexander Toshev, Vaishaal Shankar, Joshua M Susskind, and Armand Joulin. Scalable pre-training of large autoregressive image models. *arXiv preprint arXiv:2401.08541*, 2024. 1
- [9] Patrick Esser, Robin Rombach, and Björn Ommer. Taming transformers for high-resolution image synthesis. *arXiv preprint arXiv:2012.09841*, 2020. 1, 3, 5, 7, 12
- [10] Patrick Esser, Robin Rombach, and Bjorn Ommer. Taming transformers for high-resolution image synthesis. In *Proceedings of the IEEE/CVF conference on computer vision and pattern recognition*, pp. 12873–12883, 2021. 2
- [11] Patrick Esser, Sumith Kulal, Andreas Blattmann, Rahim Entezari, Jonas Müller, Harry Saini, Yam Levi, Dominik Lorenz, Axel Sauer, Frederic Boesel, et al. Scaling rectified flow transformers for high-resolution image synthesis. *arXiv preprint arXiv:2403.03206*, 2024. 13
- [12] Samir Yitzhak Gadre, Georgios Smyrnis, Vaishaal Shankar, Suchin Gururangan, Mitchell Wortsman, Rulin Shao, Jean Mercat, Alex Fang, Jeffrey Li, Sedrick Keh, et al. Language models scale reliably with over-training and on downstream tasks. *arXiv preprint arXiv:2403.08540*, 2024. 4
- [13] Robert Gray. Vector quantization. *IEEE Assp Magazine*, 1(2):4–29, 1984. 2
- [14] Yuchao Gu, Xintao Wang, Yixiao Ge, Ying Shan, Xiaohu Qie, and Mike Zheng Shou. Rethinking the objectives of vector-quantized tokenizers for image synthesis. *arXiv preprint arXiv:2212.03185*, 2022. 2
- [15] Tom Henighan, Jared Kaplan, Mor Katz, Mark Chen, Christopher Hesse, Jacob Jackson, Heewoo Jun, Tom B Brown, Prafulla Dhariwal, Scott Gray, et al. Scaling laws for autoregressive generative modeling. *arXiv preprint arXiv:2010.14701*, 2020. 2, 4
- [16] Martin Heusel, Hubert Ramsauer, Thomas Unterthiner, Bernhard Nessler, and Sepp Hochreiter. Gans trained by a two time-scale update rule converge to a local nash equilibrium. *arXiv preprint arXiv:1706.08500*, 2017. 3
- [17] Irina Higgins, Loic Matthey, Arka Pal, Christopher P Burgess, Xavier Glorot, Matthew M Botvinick, Shakir Mohamed, and Alexander Lerchner. beta-vae: Learning basic visual concepts with a constrained variational framework. *ICLR (Poster)*, 3, 2017. 3
- [18] Jonathan Ho and Tim Salimans. Classifier-free diffusion guidance. *arXiv preprint arXiv:2207.12598*, 2022. 13
- [19] Jordan Hoffmann, Sebastian Borgeaud, Arthur Mensch, Elena Buchatskaya, Trevor Cai, Eliza Rutherford, Diego de Las Casas, Lisa Anne Hendricks, Johannes Welbl, Aidan Clark, et al. Training compute-optimal large language models. *arXiv preprint arXiv:2203.15556*, 2022. 2, 13
- [20] Minyoung Huh, Brian Cheung, Pulkit Agrawal, and Phillip Isola. Straightening out the straight-through estimator: Overcoming optimization challenges in

- vector quantized networks. In *International Conference on Machine Learning*, pp. 14096–14113. PMLR, 2023. 2
- [21] Phillip Isola, Jun-Yan Zhu, Tinghui Zhou, and Alexei A Efros. Image-to-image translation with conditional adversarial networks. *arXiv preprint arXiv:1611.07004*, 2016. 12
- [22] Yang Jin, Kun Xu, Kun Xu, Liwei Chen, Chao Liao, Jianchao Tan, Quzhe Huang, Bin Chen, Chenyi Lei, An Liu, et al. Unified language-vision pretraining in llm with dynamic discrete visual tokenization. *arXiv preprint arXiv:2309.04669*, 2024. 2
- [23] Jared Kaplan, Sam McCandlish, Tom Henighan, Tom B Brown, Benjamin Chess, Rewon Child, Scott Gray, Alec Radford, Jeffrey Wu, and Dario Amodei. Scaling laws for neural language models. *arXiv preprint arXiv:2001.08361*, 2020. 2, 4, 13
- [24] Tero Karras, Samuli Laine, Miika Aittala, Janne Hellsten, Jaakko Lehtinen, and Timo Aila. Analyzing and improving the image quality of stylegan. *arXiv preprint arXiv:1912.04958*, 2019. 12
- [25] Maciej Kilian, Varun Japan, and Luke Zettlemoyer. Computational tradeoffs in image synthesis: Diffusion, masked-token, and next-token prediction. *arXiv preprint arXiv:2405.13218*, 2024. 6
- [26] Diederik P Kingma. Adam: A method for stochastic optimization. *arXiv preprint arXiv:1412.6980*, 2014. 12
- [27] Doyup Lee, Chiheon Kim, Saehoon Kim, Minsu Cho, and Wook-Shin Han. Autoregressive image generation using residual quantization. *arXiv preprint arXiv:2203.01941*, 2022. 5, 7
- [28] Brian Lester, Jaehoon Lee, Alex Alemi, Jeffrey Pennington, Adam Roberts, Jascha Sohl-Dickstein, and Noah Constant. Training llms over neurally compressed text. *arXiv preprint arXiv:2404.03626*, 2024. 3
- [29] Tianhong Li, Dina Katabi, and Kaiming He. Return of unconditional generation: A self-supervised representation generation method. In *The Thirty-eighth Annual Conference on Neural Information Processing Systems*, 2024. 7
- [30] Tianhong Li, Yonglong Tian, He Li, Mingyang Deng, and Kaiming He. Autoregressive image generation without vector quantization. *arXiv preprint arXiv:2406.11838*, 2024. 7, 13
- [31] Zhuoyan Luo, Fengyuan Shi, Yixiao Ge, Yujie Yang, Limin Wang, and Ying Shan. Openmagvit2: An open-source project toward democratizing auto-regressive visual generation. *arXiv preprint arXiv:2409.04410*, 2024. 3
- [32] Fabian Mentzer, David Minnen, Eirikur Agustsson, and Michael Tschanen. Finite scalar quantization: Vq-vae made simple. *arXiv preprint arXiv:2309.15505*, 2023. 2, 3, 5, 6
- [33] William Peebles and Saining Xie. Scalable diffusion models with transformers. *arXiv preprint arXiv:2212.09748*, 2022. 7
- [34] Z Peng, L Dong, H Bao, Q Ye, and F Wei. Beit v2: Masked image modeling with vector-quantized visual tokenizers. *arXiv preprint arXiv:2208.06366*, 2022. 2
- [35] Alec Radford. Improving language understanding by generative pre-training. 2018. 1
- [36] Alec Radford, Jong Wook Kim, Chris Hallacy, Aditya Ramesh, Gabriel Goh, Sandhini Agarwal, Girish Sastry, Amanda Askell, Pamela Mishkin, Jack Clark, et al. Learning transferable visual models from natural language supervision. In *International conference on machine learning*, pp. 8748–8763. PMLR, 2021. 6
- [37] Ali Razavi, Aaron van den Oord, and Oriol Vinyals. Generating diverse high-fidelity images with vq-vae-2. *arXiv preprint arXiv:1906.00446*, 2019. 7
- [38] Anton Razhigaev, Arseniy Shakhmatov, Anastasia Maltseva, Vladimir Arkhipkin, Igor Pavlov, Ilya Ryabov, Angelina Kuts, Alexander Panchenko, Andrey Kuznetsov, and Denis Dimitrov. Kandinsky: an improved text-to-image synthesis with image prior and latent diffusion. *arXiv preprint arXiv:2310.03502*, 2023. 2
- [39] Juan A Rodriguez, David Vazquez, Issam Laradji, Marco Pedersoli, and Pau Rodriguez. Ocr-vqgan: Taming text-within-image generation. In *Proceedings of the IEEE/CVF Winter Conference on Applications of Computer Vision*, pp. 3689–3698, 2023. 2
- [40] Robin Rombach, Andreas Blattmann, Dominik Lorenz, Patrick Esser, and Björn Ommer. High-resolution image synthesis with latent diffusion models. *arXiv e-prints*, pp. arXiv–2112, 2021. 1, 7
- [41] Olga Russakovsky, Jia Deng, Hao Su, Jonathan Krause, Sanjeev Satheesh, Sean Ma, Zhiheng Huang, Andrej Karpathy, Aditya Khosla, Michael Bernstein, et al. Imagenet large scale visual recognition challenge. *arXiv preprint arXiv:1409.0575*, 2014. 2
- [42] Craig W Schmidt, Varshini Reddy, Haoran Zhang, Alec Alameddine, Omri Uzan, Yuval Pinter, and Chris Tanner. Tokenization is more than compression. *arXiv preprint arXiv:2402.18376*, 2024. 3
- [43] Peize Sun, Yi Jiang, Shoufa Chen, Shilong Zhang, Bingyue Peng, Ping Luo, and Zehuan Yuan. Autoregressive model beats diffusion: Llama for scalable image generation. *arXiv preprint arXiv:2406.06525*, 2024. 2, 3, 4, 5, 7, 12, 13
- [44] Christian Szegedy, Wei Liu, Yangqing Jia, Pierre Sermanet, Scott Reed, Dragomir Anguelov, Dumitru Erhan, Vincent Vanhoucke, and Andrew Rabinovich.

- Going deeper with convolutions. In *Proceedings of the IEEE conference on computer vision and pattern recognition*, pp. 1–9, 2015. 3
- [45] Keyu Tian, Yi Jiang, Zehuan Yuan, Bingyue Peng, and Liwei Wang. Visual autoregressive modeling: Scalable image generation via next-scale prediction. *arXiv preprint arXiv:2404.02905*, 2024. 7, 13
- [46] Hugo Touvron, Thibaut Lavril, Gautier Izacard, Xavier Martinet, Marie-Anne Lachaux, Timothée Lacroix, Baptiste Rozière, Naman Goyal, Eric Hambro, Faisal Azhar, et al. Llama: Open and efficient foundation language models. *arXiv preprint arXiv:2302.13971*, 2023. 1, 12, 13
- [47] Michael Tschannen, Olivier Bachem, and Mario Lucic. Recent advances in autoencoder-based representation learning. *arXiv preprint arXiv:1812.05069*, 2018. 3
- [48] Michael Tschannen, Cian Eastwood, and Fabian Mentzer. Givt: Generative infinite-vocabulary transformers. In *European Conference on Computer Vision*, pp. 292–309. Springer, 2025. 3
- [49] Aaron Van Den Oord, Oriol Vinyals, et al. Neural discrete representation learning. *Advances in neural information processing systems*, 30, 2017. 2, 12
- [50] Junke Wang, Yi Jiang, Zehuan Yuan, Binyue Peng, Zuxuan Wu, and Yu-Gang Jiang. Omnitokenizer: A joint image-video tokenizer for visual generation. *arXiv preprint arXiv:2406.09399*, 2024. 2
- [51] Luting Wang, Yang Zhao, Zijian Zhang, Jiashi Feng, Si Liu, and Bingyi Kang. Image understanding makes for a good tokenizer for image generation. *arXiv preprint arXiv:2411.04406*, 2024. 2
- [52] Fisher Yu, Ari Seff, Yinda Zhang, Shuran Song, Thomas Funkhouser, and Jianxiong Xiao. Lsun: Construction of a large-scale image dataset using deep learning with humans in the loop. *arXiv preprint arXiv:1506.03365*, 2015. 2, 6
- [53] Jiahui Yu, Xin Li, Jing Yu Koh, Han Zhang, Ruoming Pang, James Qin, Alexander Ku, Yuanzhong Xu, Jason Baldridge, and Yonghui Wu. Vector-quantized image modeling with improved vqgan. *arXiv preprint arXiv:2110.04627*, 2021. 2, 5, 7, 12
- [54] Jiahui Yu, Yuanzhong Xu, Jing Yu Koh, Thang Luong, Gunjan Baid, Zirui Wang, Vijay Vasudevan, Alexander Ku, Yinfei Yang, Burcu Karagol Ayan, et al. Scaling autoregressive models for content-rich text-to-image generation. *arXiv preprint arXiv:2206.10789*, 2(3):5, 2022. 1, 3
- [55] Lijun Yu, José Lezama, Nitesh B Gundavarapu, Luca Versari, Kihyuk Sohn, David Minnen, Yong Cheng, Vighnesh Birodkar, Agrim Gupta, Xiuye Gu, et al. Language model beats diffusion—tokenizer is key to visual generation. *arXiv preprint arXiv:2310.05737*, 2023. 3, 5
- [56] Lili Yu, Bowen Shi, Ramakanth Pasunuru, Benjamin Muller, Olga Golovneva, Tianlu Wang, Arun Babu, Binh Tang, Brian Karrer, Shelly Sheynin, et al. Scaling autoregressive multi-modal models: Pretraining and instruction tuning. *arXiv preprint arXiv:2309.02591*, 2(3), 2023. 13
- [57] Qihang Yu, Mark Weber, Xueqing Deng, Xiaohui Shen, Daniel Cremers, and Liang-Chieh Chen. An image is worth 32 tokens for reconstruction and generation. *arXiv preprint arXiv:2406.07550*, 2024. 2
- [58] Richard Zhang, Phillip Isola, Alexei A Efros, Eli Shechtman, and Oliver Wang. The unreasonable effectiveness of deep features as a perceptual metric. In *Proceedings of the IEEE conference on computer vision and pattern recognition*, pp. 586–595, 2018. 2, 12
- [59] Susan Zhang, Stephen Roller, Naman Goyal, Mikel Artetxe, Moya Chen, Shuohui Chen, Christopher Dewan, Mona Diab, Xian Li, Xi Victoria Lin, et al. Opt: Open pre-trained transformer language models. *arXiv preprint arXiv:2205.01068*, 2022. 2
- [60] Yue Zhao, Yuanjun Xiong, and Philipp Krähenbühl. Image and video tokenization with binary spherical quantization. *arXiv preprint arXiv:2406.07548*, 2024. 2
- [61] Chuanxia Zheng, Tung-Long Vuong, Jianfei Cai, and Dinh Phung. Movq: Modulating quantized vectors for high-fidelity image generation. *Advances in Neural Information Processing Systems*, 35:23412–23425, 2022. 2, 5
- [62] Zhenhai Zhu and Radu Soricut. Wavelet-based image tokenizer for vision transformers. *arXiv preprint arXiv:2405.18616*, 2024. 2

# Supplementary Material

**Structure of Appendix.** Appendix A documents full training details for all experiments and architectures. Appendix B discusses the limitations of our experimental methodology. Appendix C provides more detailed scaling analysis across a range of experiments in the main paper. Appendix D (Figures 15-19) provides non-cherry-picked qualitative generations across a range of ImageNet categories for our best model.

## A. Further training details

In this section, we enumerate the complete training details for experiments in Section 3. These basic hyperparameters are the same for both

### A.1. Stage 1: VQGAN training

We largely follow the training recipes from [9] and [43] to train our tokenizer, with modifications that we state here. The VQGAN architecture is exactly that of [9], with the following standard loss terms (not including our CRT loss):

$$\mathcal{L} = \lambda_{VQ}\mathcal{L}_{VQ} + \lambda_{GAN}\mathcal{L}_{GAN} + \lambda_{Perceptual}\mathcal{L}_{Perceptual} + \lambda_{L2}\mathcal{L}_2. \quad (1)$$

The perceptual loss comes from LPIPS [58]. The  $\ell_2$  loss is defined as  $\mathcal{L}_2(x, y) = \|x - y\|_2^2$  between the reconstruction and the input. The weights for each loss are:  $\lambda_{VQ} = 1.0$ ,  $\lambda_{GAN} = 0.5$ ,  $\lambda_{Perceptual} = 1.0$ ,  $\lambda_{L2} = 1.0$ . We start  $\lambda_{GAN}$  at 0. After 20k iterations, we anneal  $\lambda_{GAN}$  to 0.5 using a cosine schedule for 2k iterations.

**GAN Loss Details.** The GAN loss uses the PatchGAN [21] as a discriminator with the Wasserstein GAN loss function from [2] directly on reconstructions from the auto-encoder to force the output to look “realistic.” This is the only “reference-free” image loss used. Using improved StyleGAN and StyleGAN2 [24] discriminators ended up with worse qualitative results in our setting.

**Codebook Loss Details.** Following [43, 53], we project from 256 to 8 dimensions before doing codebook lookup and perform codebook lookup with cosine distance. We use two losses, a quantization error loss and a commitment loss, both proposed in [49], with a commitment  $\beta = 0.25$ . We do not use entropy loss, as it was unnecessary to prevent codebook collapse in our setup. We find that training with a long learning rate warmup period is crucial for scaling beyond 16k codes, otherwise performance saturates at 2.1 rFID and codebook utilization stagnates.

**Optimization Parameters.** We use Adam [26] with learning rate  $1e - 4$  and  $\beta = (0.9, 0.95)$ . AdamW with weight decay 0.1 performs identically. We use the same optimization parameters for the PatchGAN discriminator. We use

with linear warmup from  $1e - 5$  for 3k iterations, batch size 128 and a constant learning rate. We found that this warmup is critical for good performance, especially for codebook length and training duration scaling. Cosine learning rate gave very similar results, and constant learning rate allows for continued training. We train for a total of 400k iterations unless stated otherwise.

**CRT details.** CRT is our L2 next-token prediction loss applied to the raster-order tokens during stage 1 training. The weight for this loss for all of our experiments is 4.0 (we include a sweep in Figure 9) Like with the GAN discriminator, we anneal this weight from 0 to 4.0 for 1k iterations from the start of training. The duration of this annealing is not important for final performance. The architecture we use is identical to our stage 2 model, except with no last classification layer and no token embedding layer (replaced with a single linear layer). We use a separate optimizer for this component: an AdamW optimizer with learning rate and  $\beta$  parameters matching the original VQGAN at all iterations. Our weight decay was 0.1. We normalize the loss by the annealed weight at all iterations so that the causal model training is not impacted by its weight. To control for extra training FLOPs, we drop the number of training iterations to 380k. For CRT<sub>opt</sub>, we train for 800k iterations.

### A.2. Stage 2: Auto-regressive training

**Architecture.** Following [43], we use the Llama 2 architecture [46] with QK-layer normalization [5] for stability. For some 576 tokens/image runs, we also needed to use z-loss [4?] with a coefficient of  $1e - 4$  for stability. We find that this did not impact the performance of stable runs. The

**Optimization.** We perform data augmentation using ten-crop, allowing us to pre-tokenize the train set during stage 2 training. We use AdamW, betas (0.9, 0.95) and a cosine learning with schedule with a linear warmup (5k iterations) and a batch size of 256. Our max learning rate is  $3e - 3$ , with a pre-warmup learning rate of  $3e - 4$ , annealing our learning rate to 0. We also include a class token dropout rate of 0.1, where we replace the class-token with a randomly initialized learnable dummy token to enable classifier-free guidance. We train for a total of 375k iterations unless otherwise stated (we often sweep this parameter for stage 2 scaling law experiments).

**Class-conditioning and Classifier-Free Guidance (CFG).** For class-conditioning, we prepend a special class token to image token sequences at train time. At inference time, we use the relevant class token to start the sequence to generate an image of a particular class. We sample with next-token

Table 4. **Stage 2 model configurations.** These are the parameters for the Llama architectures we use in our stage 2 experiment sweeps. To construct this sweep, we interpolated by head and layer counts with existing standard models (-S, -M, -L, etc.) and ensured 64 dimensions per head.

Parameters	Heads	Layers	Dimension
$5.21 \times 10^7$	10	6	640
$8.06 \times 10^7$	11	9	704
$1.11 \times 10^8$	12	12	768
$2.12 \times 10^8$	14	18	896
$3.43 \times 10^8$	16	24	1024
$5.17 \times 10^8$	18	30	1152
$7.75 \times 10^8$	20	36	1280

prediction without top- $k$  or top- $p$  sampling. All our results use CFG at inference time to further emphasize classifier guidance. To do this, we have two inference procedures, one with the class-token and one using the aforementioned dummy token. At each timestep, these yield logits  $\ell_u$  for the unconditional logit, and  $\ell_c$  for the class-conditioned logit. To get the next token, we sample from the combined logit  $\ell_{cfg} = \ell_u + (\ell_c - \ell_u)\alpha$ , where  $\alpha$  is known at the CFG scale. This kind of sampling was initially used for diffusion [18], but has seen success in auto-regressive image generation as well [43, 56] and is used commonly.

CFG trades off fidelity and diversity (related to precision and recall respectively) of generation, and we found that the optimal CFG scale was also pareto optimal for precision and recall. To choose our CFG scale at inference time, we split a 50k subset of the train set (not held out during training) to compute FID against. We select the optimal FID against samples from  $\alpha \in \{1.5, 1.75, 2.0, 2.25\}$  and use those generations against the validation set. We do this because CFG can have a large effect on FID score [30, 43, 45], and optimizing directly against the ImageNet validation set can pollute our evaluation. However, in separate experiments, we find that optimal CFG against this train split and the validation set are identical in practice.

### A.3. Scaling law sweep details

To produce scaling laws (e.g. Figure 3), we sweep training compute by changing the number of total training iterations. Because we are in the repeated data setting, unlike [23], and we are using a cosine learning rate schedule, we need to evaluate the end points of separate, independent training runs to produce these curves. The iteration counts we sweep over are  $\{15k, 22.5k, 45k, 90k, 187.5k, 375k, 750k, 1.5M, 2.25M\}$  for all models. We compute estimates for training FLOPs using the approximation from [23]. The architecture parameters for our sweep can be found in Table 4.

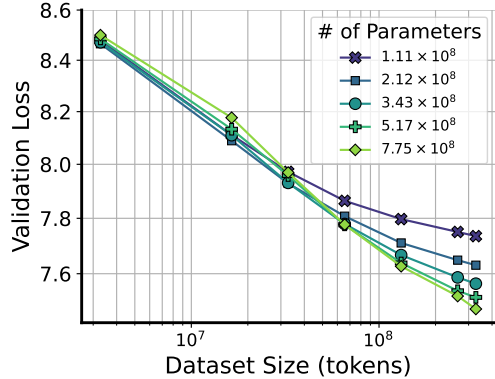


Figure 11. **Stage 2 Validation Loss by Dataset Size.** Here we study the data scale bottleneck by varying the total size of the dataset. Every model was trained for 250k iterations at batch size 256. We see that our dataset is large enough to demonstrate scaling laws at the parameter range studied.

## B. Limitations

Our work has a few specific limitations, largely related to the availability of compute. First, the largest model we test is 775M, which we do in order to prevent overfitting. This is close to the range of current state-of-the-art image generation models, such as [11] which ranges from 800M parameters to 8B parameters, but is smaller than modern large language models [19, 46]. Future work could include scaling parameter counts. Second, we primarily evaluate on class-to-image synthesis and not text-to-image synthesis. We do this because FID is a much more well-behaved metric on ImageNet (see inconsistent scaling in LSUN results by parameter count in Table 3). However, this means we cannot train on web-scale datasets, and thus are in the repeated data regime, deviating from [23]. In Figure 11, we study the effects of this but varying the stage 2 training set size (375k training iterations), showing that for existing model sizes we are not yet in the data bottleneck regime. Future work could include validating an in distribution metric (e.g. CLIP FID) on a large scale text-to-image dataset and then reproducing our scaling laws.

## C. More Detailed Scaling Plots

In this section we cover more detailed scaling law explorations expanding on plots in the main paper.

Figure 13 expands on Figure 7, showing full model size scaling details and best fit scaling laws. We see the same trends discussed in the original plot, where 1k performs better in low regimes and 131k performs better in high compute regimes.

Figure 14 expands on Figure 4, showing scaling across three different tokens per image amounts on all of our model scales. We see the same trend but in more detail, where 576

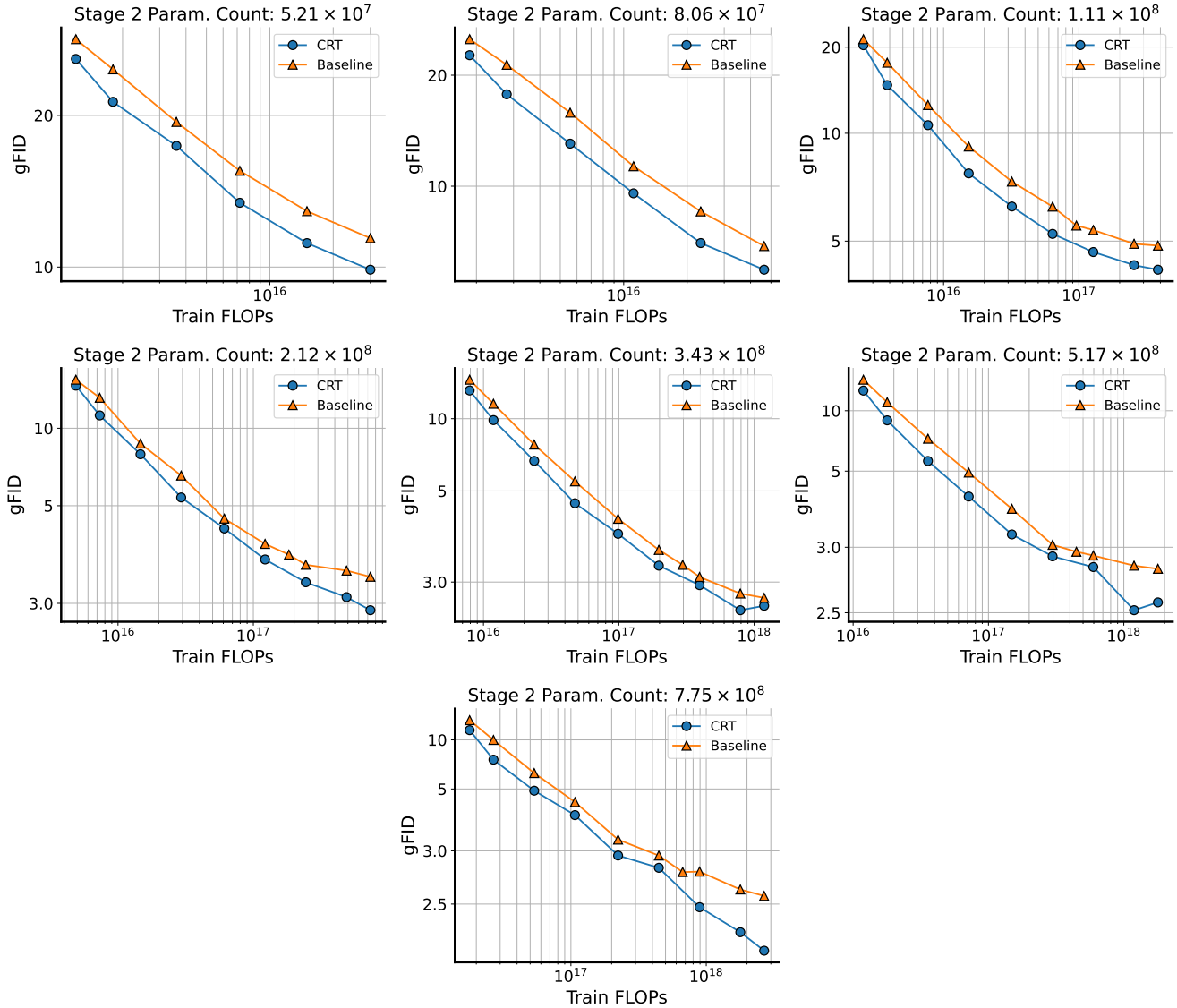


Figure 12. **Individual model scale comparison for Figures 3 and 8.** Here we show how stage 2 gFID scales with respect to train FLOPs with both the CRT and baseline tokenizer. We see that with CRT tokens, stage 2 learns faster and also ends up more performant across all model sizes, especially at smaller scales (note the log-scaled y-axis).

performs poorly in low compute regimes (and with small models) but outperforms 400 and 256 tokens per image at high compute regimes. Note that 256 tokens per image is compute optimal up until the 2.5 gFID barrier is reached, at which point the tokenizer reconstruction quality becomes a bottleneck.

Figure 12 provides a different perspective on the comparison between Figures 3 and 8. We do this by comparing stage 2 model scales directly by gFID performance by train FLOPs. Note that like the main figure, each point is an independent training run. We see that CRT tokens improve performance at all scales both for training efficiency and fi-

nal performance. This difference is especially pronounced at the smaller compute and parameter scales.

#### D. Qualitative Examples

Figures 15-19 show non-cherry-picked generation examples from our best model  $\text{CRT}_{opt}\text{-AR-775M}$ . They demonstrate a high degree of diversity and image quality across a wide array of classes.

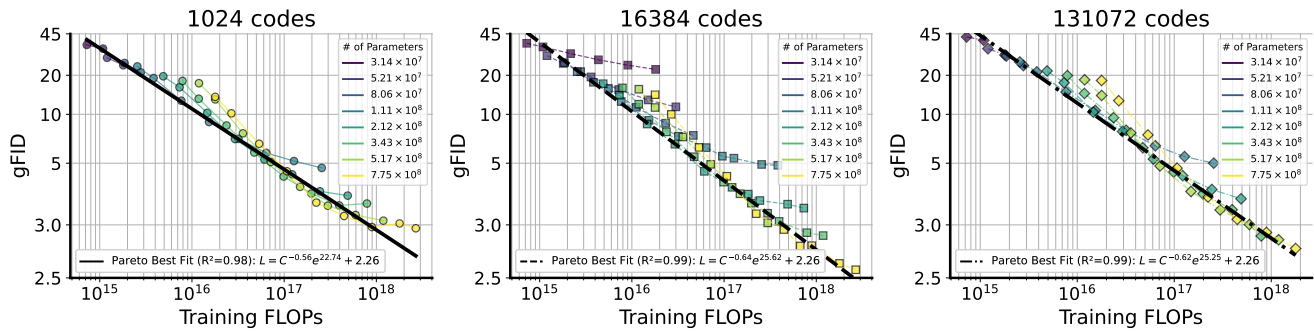


Figure 13. **Full scaling law plots for Pareto curves from Figure 7.** Here we show individual model scaling (similar to Figure 3) at three different stage 1 codebook sizes. 1k outperforms 131k at low compute regimes and the trend reverses at high compute regimes. Note that 16k outperforms both even though it has worse rFID than the 131k codebook size tokenizer (2.21 rFID vs 1.72 rFID).

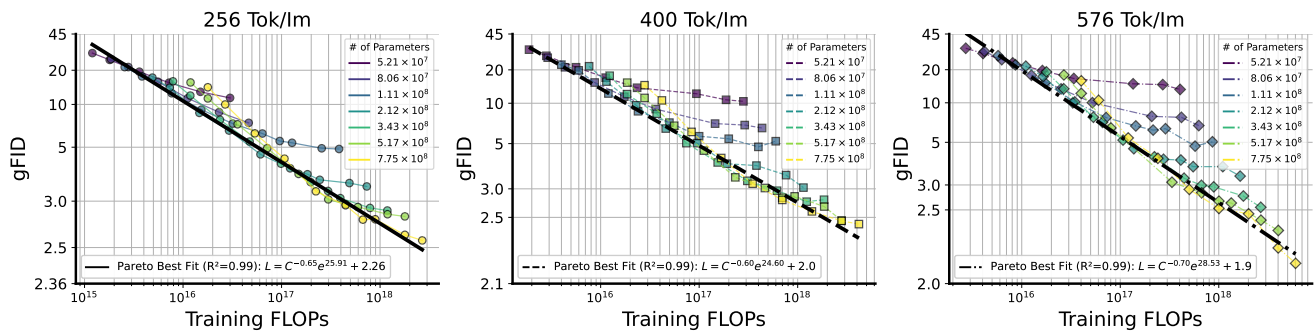


Figure 14. **Full scaling law plots for tokens per image scaling exploration (Figure 4).** Here we show individual model scaling (similar to Figure 3) at three different tokens per image values. We see the same trend but in more detail, where 576 performs poorly in low compute regimes (and with small models) but outperforms 400 and 256 tokens per image at high compute regimes. Note that 256 tokens per image is compute optimal up until the 2.5 gFID barrier is reached, at which point the tokenizer reconstruction quality becomes a bottleneck.

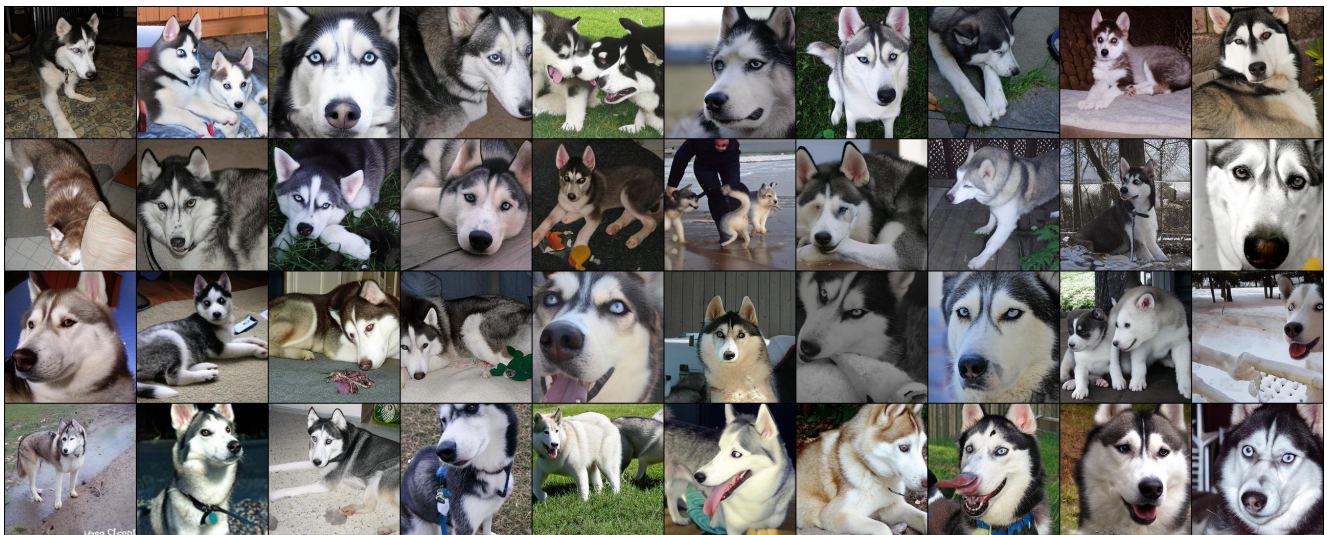


Figure 15. **Non-cherry-picked generation examples from CRT<sub>opt</sub>-AR-775M (ImageNet 256x256).** CFG scale = 2.0, class index 250, class name Siberian Husky

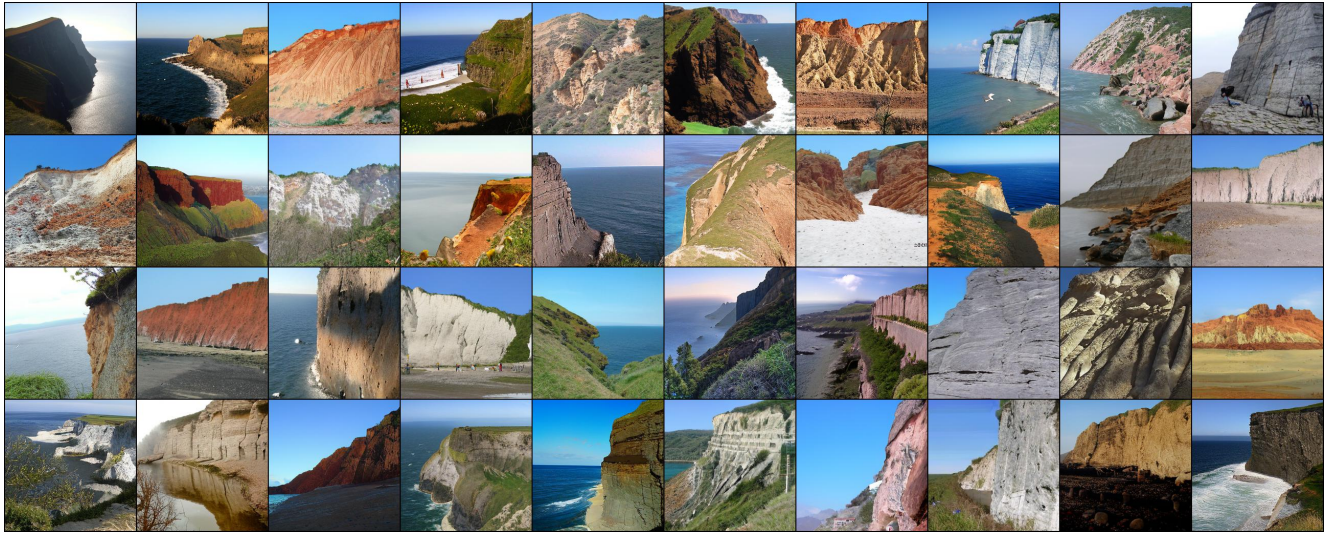


Figure 16. Non-cherrypicked generation examples from  $CRT_{opt}$ -AR-775M (ImageNet 256x256). CFG scale = 2.0, class index 972, class name cliff



Figure 17. Non-cherrypicked generation examples from  $CRT_{opt}$ -AR-775M (ImageNet 256x256). CFG scale = 2.0, class index 207, class name Golden Retriever





Figure 18. Non-cherrypicked generation examples from CRT<sub>opt</sub>-AR-775M (ImageNet 256x256). CFG scale = 2.0, class index 90, class name lorikeet



Figure 19. Non-cherrypicked generation examples from CRT<sub>opt</sub>-AR-775M (ImageNet 256x256). CFG scale = 2.0, class index 29, class name axolotl



Figure 20. Non-cherrypicked generation examples from  $CRT_{opt}$ -AR-775M (ImageNet 256x256). CFG scale = 2.0, class index 297, class name sloth bear



Figure 21. Non-cherrypicked generation examples from  $CRT_{opt}$ -AR-775M (ImageNet 256x256). CFG scale = 2.0, class index 248, class name husky

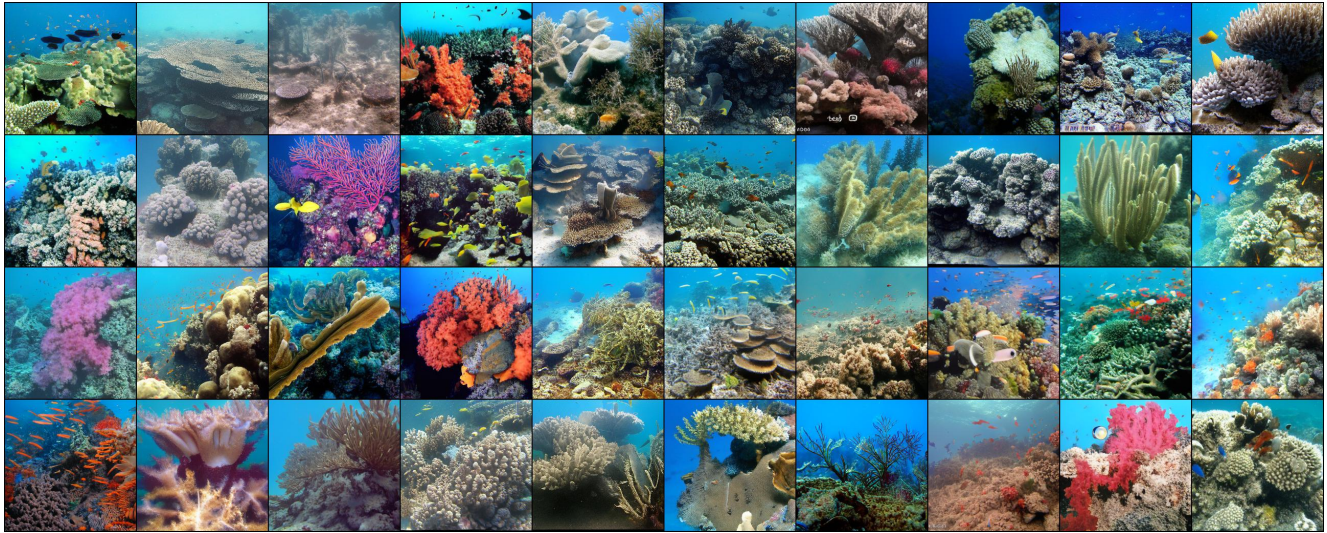


Figure 22. Non-cherrypicked generation examples from  $CRT_{opt}$ -AR-775M (ImageNet 256x256). CFG scale = 2.0, class index 973, class name coral reef



Figure 23. Non-cherrypicked generation examples from  $CRT_{opt}$ -AR-775M (ImageNet 256x256). CFG scale = 2.0, class index 993, class name gyromitra



Figure 24. Non-cherrypicked generation examples from  $CRT_{opt}$ -AR-775M (ImageNet 256x256). CFG scale = 2.0, class index 388, class name giant panda



Figure 25. Non-cherrypicked generation examples from  $CRT_{opt}$ -AR-775M (ImageNet 256x256). CFG scale = 2.0, class index 387, class name red panda



Figure 26. Non-cherrypicked generation examples from  $CRT_{opt}$ -AR-775M (ImageNet 256x256). CFG scale = 2.0, class index 417, class name balloon



Figure 27. Non-cherrypicked generation examples from  $CRT_{opt}$ -AR-775M (ImageNet 256x256). CFG scale = 2.0, class index 279, class name Arctic fox



Figure 28. Non-cherrypicked generation examples from  $CRT_{opt}$ -AR-775M (ImageNet 256x256). CFG scale = 2.0, class index 291, class name lion